IX International Conference on Particle-Based Methods
PARTICLES 2025
J. Bonet, M. Cremonesi, A. Franci, A. Gil (Eds)

METHODS 3D DEM INVESTIGATION INTO THE LIQUEFACTION CHARACTERISTICS OF HIGHLY CRUSHABLE PUMICE SAND

SAYED H. BAHMANI[*], ROLANDO P. ORENSE[†], ZEINAB BAKHSHIPOUR[‡] AND INTAN BAHRI[*]

[*] Department of Civil Engineering
Unitec Institute of Technology
Campus Mount Albert, 1025 Auckland, New Zealand
e-mail: sbahmani@unitec.ac.nz, www.unitec.ac.nz

[†] University of Auckland
Engineering Block 1, Campus Auckland
20 Symonds St, 1010 Auckland, New Zealand
email: r.orense@auckland.ac.nz, www.auckland.ac.nz

[‡] Chambers Consultants Limited
39 East Tamaki Road, Papatoetoe,
2025 Auckland, New Zealand
email: azi@chambersconsultants.co.nz, www.chambersconsultants.co.nz

Key words: Liquefaction, Pumice, Sand, Distinct Element Model, Crushing, Cyclic.

Abstract. Pumice sand particles present engineering challenges due to their tendency to crush and compress. Although laboratory and field tests can assess their behaviour, these methods are often time-consuming and costly. This study investigates the liquefaction behaviour of crushable pumice sand using the Discrete Element Method (DEM). In the model, each pumice particle is represented as a sphere that fractures into 14 smaller spheres when a critical contact force is exceeded. Initially, single particle crushing tests are conducted to determine breakage characteristics based on particle size. Subsequently, using the open-source code YADE, three-dimensional loose specimens are prepared and isotopically consolidated under specified confining pressures. These numerical specimens undergo cyclic loading under undrained conditions. The findings indicate that the DEM model successfully replicates experimental results, providing insights into how particle crushing influences cyclic deviator strain. Microscale observations also shed light on the development of force chains within the specimens, enhancing the understanding of pumice sand behaviour during cyclic loading.

1 INTRODUCTION

Volcanic activity in the Taupo Volcanic Zone has led to widespread deposition of pumiceous materials across the central North Island of New Zealand. These deposits are especially prevalent in river valleys and floodplains, making them a common feature in local engineering projects. As such, understanding their geotechnical behaviour is of significant importance.

Pumice sands, in particular, present unique challenges due to their highly crushable, compressible, and lightweight nature, which stems from their vesicular (bubble-like) internal structure. These traits differentiate them from conventional quartz-based sands and complicate the use of standard engineering correlations and analysis techniques.

To better understand these materials, the Geomechanics Group at the University of Auckland has conducted a range of investigations, including calibration chamber tests and other laboratory-based element tests (e.g., Wesley et al., 1999; Pender et al., 2006; Orense et al., 2012; Kikkawa et al., 2013). While these studies have provided valuable insights, further testing is needed to fully characterise pumice sand behaviour—though such physical testing can be both costly and time-intensive.

To overcome these limitations, this study explores the use of the Discrete Element Method (DEM) as a supplementary or alternative tool. DEM enables simulation of particle-scale behaviour using data from laboratory and field observations, providing a means to observe both macro- and micro-scale responses that are otherwise difficult or impractical to measure directly (Cundall, 1988). Numerous researchers have used DEM to study the mechanical behaviour of granular materials under various loading conditions (e.g., Belheine et al., 2009; Cil & Alshibli, 2014; Gong et al., 2012; O'Sullivan, 2011).

This paper applies DEM to examine the undrained cyclic behaviour of pumice sand in triaxial tests, focusing on materials highly crushable that they can be crushed by a fingernail. The open-source platform YADE is employed for its adaptability, allowing for the customisation of contact laws and particle geometries via object-oriented scripting (Šmilauer et al., 2010). The DEM models are calibrated and validated using experimental data from physical pumice sand tests. This study aims to deepen the qualitative understanding of crushable granular materials by exploring their micro-mechanical behaviour.

2 PARTICLE CRUSHING

2.1 Single particle crushing tests

To examine how the particle strength varies with the size of the particle, single particle crushing tests were conducted on pumice particles with nominal sizes ranging from 1 – 8 mm. Approximately 30 particles were tested for each nominal size. The results obtained were consistent with those reported by Orense et al. (2013), which showed that the particle crushing strength, σ_c, decreases with increasing particle size, d. The results are then expressed in terms of probability of the particle surviving the crushing, Ps, as a function of crushing strength, σc (see Figure 1). Next, the statistical model originally formulated by Weibull (1951) and extended by McDowell and Bolton (1998) was used to represent the probability of survival, Ps, i.e.

$$P_s(d) = \exp\left[-\left(\frac{d}{d_0}\right)^3 \left(\frac{\sigma_c}{\sigma_0}\right)^m\right] \quad (1)$$

where σ_0 is the crushing strength at which 37% of the tested particles survive and is approximately equal to the mean tensile strength of particles of size d_0. In Eq (1), m is the Weibull modulus, which can be described as a shape parameter for the Weibull distribution model, i.e., high value indicates little strength variation from particle to particle. The results of the analysis show that for pumice sand, m=1.17, much lower than those reported in the literature for various granular materials, indicating that physical flaws (such as surface and internal voids)

within the particles are clustered inconsistently, and the measured strength is broadly distributed.

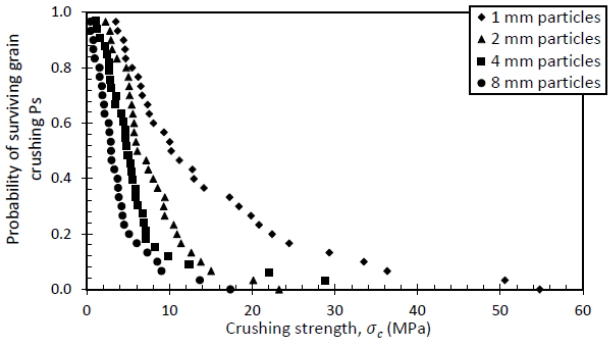

Figure 1: Probability of survival (Weibull distribution) considering the crushing strength for four different pumice particle sizes.

2.1 Particle crushing criteria

In the DEM, the failure criteria adopted are based on the approach of Russell et al. (2009) considering the Von Mises criterion. Here, a particle subject to several external force points may crush when the applied force, F, exceeds the following limit conditions:

$$F \leq \sigma_{lim}.A_F \tag{2}$$

where σ_{lim} is the particle strength limit, and AF is the contact area. The particle strength limit is assumed to be normally distributed for a particular particle size d, whose mean strength factor, $\bar{\sigma}_{lim}$is given by:

$$\bar{\sigma}_{lim} = \sigma_{lim0}.f(Var)(\frac{d}{d_0})^{-3/m} \tag{3}$$

where σ_{lim0} is the mean limit strength of a particle with diameter d0, and f(var) represents the influence of the particle strength variation. The following expression can be obtained by using the linear contact theory Ciantia et al., (2019):

$$F \leq \left\{ \sigma_{lim0}.f(Var)\left(\frac{d}{d_0}\right)^{-\frac{3}{m}} \pi \left[\frac{3}{4} \frac{(\frac{1-v_A^2}{E_A} + \frac{1-v_B^2}{E_B}}{\left(\frac{1}{r_A} + \frac{1}{r_B}\right)} \right]^{2/3} \right\}^3 \tag{4}$$

where r_A and r_B are the radii of the contacting spheres, and Ei and i are the Young's moduli and Poisson's ratios, respectively. Note that this basic criterion does not only relate strictly to maximum force on the particle but also to the characteristics of the contacting particles. Once the limit condition is reached, a spherical particle will split into smaller, inscribed tangent spheres. Ciantia et al. (2015) detailed the procedure involved and reported that the 14-ball splitting configuration, shown in Figure 2, is accurate enough to simulate the macroscopic behaviour. After crushing, exemplified by the splitting of the smaller spheres, the daughter fragments assume the velocity and material parameters of the mother particle, except for the intrinsic strength (σ_{lim0}), which is randomly distributed among the particles.

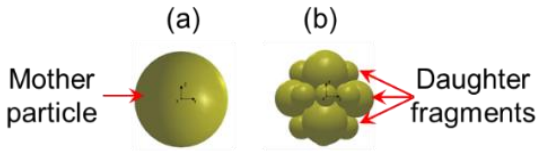

Figure 2: Modelling particle crushing in DEM: (a) original particle; (b) particle splitting configuration.

3 DEM MODELLING

3.1 DEM specimen preparation and testing

Cubical sand specimens (10 mm × 10 mm × 20 mm), each comprising 10,000 spherical particles, were prepared at the pre-defined relative densities, as shown in Figure 3. While the specimens have particle size distributions which were the same as those used in the actual experiments, the figure represents the particle sizes in terms of different colours, i.e., blue represents the smaller sizes while the red shows the bigger sizes.

The specimens were initially created using the radius expansion method (REM), where the particles were randomly placed within the target specimen volume without any locked-in force or overlap Ciantia et al., 2015). The particles are then slowly expanded until the desired radii are reached, while maintaining a constant consolidation pressure on the boundaries. During the expansion process, the evolution of the contact force between two particles causes the particles to move and rotate, allowing the boundary positions to change accordingly to maintain equilibrium for a specimen in its target state. Once the desired radii have been achieved, the inter-particle friction coefficient is reset to the expected value. The details of the input parameters are found in Table 1.

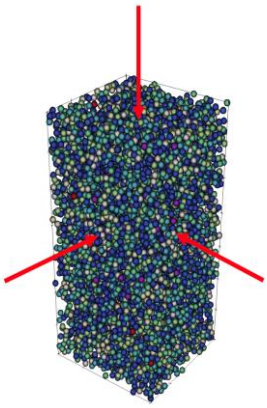

Figure 3: DEM model of triaxial specimen during consolidation with REM.

While various types of contact models are available in YADE, this study made use of the non-linear contact model, which adheres to the Hertz-Mindlin law. Here, a non-linear relationship is utilised between the normal force and the allowable shear force. The model describes the constitutive behaviour in normal and tangential directions between particles at their contact interface by adopting linear springs with normal and shear stiffnesses (Cundall, 1988). A rolling resistance model, based on the formulation of Iwashita and Oda (1998), was incorporated to simulate the surface roughness of pumice particles.

Table 1: DEM input parameters

Parameters	Value	Unit
Specimen dimensions	10×10×20	mm3
Number of particles	12,000	
Friction coefficient, μ	0.7	
Young's modulus, E	30	MPa
Poisson's ratio, ν	0.25	
Rolling stiffness coefficient, β	0.1	
ss	0.125	
Twist stiffness coefficient, Ktw	3	
Twisting strength, Twist	3	
Density	2000	kg/m3
Young's modulus of the wall	80	MPa
Poisson's ratio of the wall	0.35	
Strain rate	0.1	s^{-1}

In this study, all the presented results in this chapter are based on the strain-controlled undrained cyclic triaxial tests subjected to different values for cyclic deviator strain from ±4% to ±0.2%. The volume was kept constant while maintaining an axial strain rate of 0.1 s^{-1} and a strain rate of 0.05 s^{-1} in the two orthogonal directions. Moreover, the total stress path during cyclic shearing and pore water pressure are unknown in the DEM experiments under constant volume conditions. The assembly was considered liquefied when the ratio between the average effective stress for the assembly P_0 and the initial confining pressure P_0 decreased to 0.01.

3.2 DEM simulation of cyclic undrained triaxial tests for hard-grained sands

The undrained cyclic behaviour of sand specimens under strain-controlled mode, as reported by Kumar et al. (2017), is simulated using DEM to get better insights into the behaviour of the tested sand. Figure 4 shows the experiments and simulations in terms of axial strain, deviatoric stress, pore water pressure, and stress and strain with respect to the axial strain for a sand specimen (relative density, Dr=30%) under two levels of confining pressure (σ'_0=100).

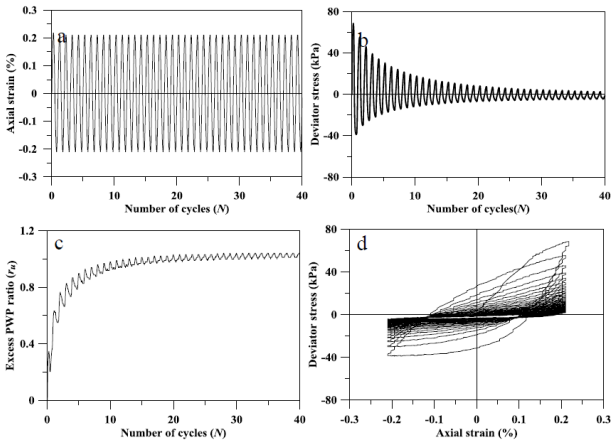

Figure 4: Laboratory results of cyclic undrained triaxial tests at 20% strain with 1 Hz frequency and 100 kPa confining pressure: (a) axial strain vs. number of cycles, (b) deviatoric stress vs. number of cycles, (c) pore water pressure vs. number of cycles, and (d) stress vs. strain (Kumar et al., 2017).

For model verification, simulated cyclic triaxial compression tests were conducted on a loose (e_0 = 2.0 or Dr = 30%) specimen with uncrushable particles under a confining pressure of 100 kPa. As shown in Figure 5, the DEM results are compared with the experimental results presented by Kumar et al. (2017), which involved cyclic triaxial compression tests conducted on sand under a strain-control mode (Figure 4).

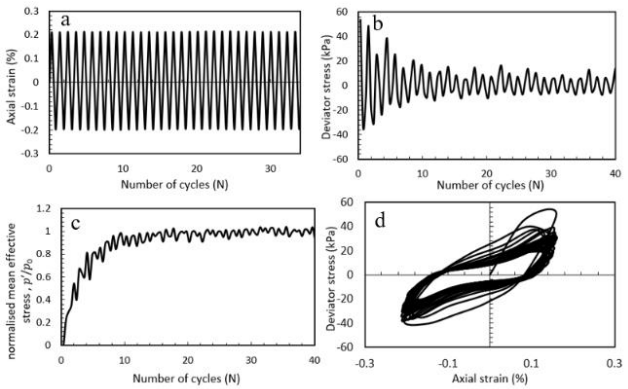

Figure 5: DEM results of cyclic undrained triaxial tests (uncrushable particles) with 1 Hz frequency and 100 kPa confining pressure for lab verification.

The results from the simulated cyclic undrained triaxial tests with a cyclic strain ratio of 0.2% and a 100 kPa confining pressure are similar to the experimental results shown in Figure 5. Under the cyclic strain-controlled amplitude, the deviatoric stress slowly decreases from 60 kPa to below 10 kPa due to the increases in the normalised mean effective stress ($\frac{p'}{p_0}$), which is used as the EPWP. In addition, normalised mean effective stress development reaches 0.95 at approximately 13 cycles, which is defined here as liquefaction. Similar behaviour is captured by DEM simulation, in which the sample liquefies at 13 cycles.

3.3 DEM simulation of cyclic undrained triaxial tests for pumice sands

In the next step, the DEM simulation was carried out using a loose pumice sand specimen (Dr=30%). The response of pumice sand is numerically modelled in this section using a non-linear contact model. The simulation was carried out in three primary stages. In this analysis, the model generated based on the initial PSD is shown in Figure 6.

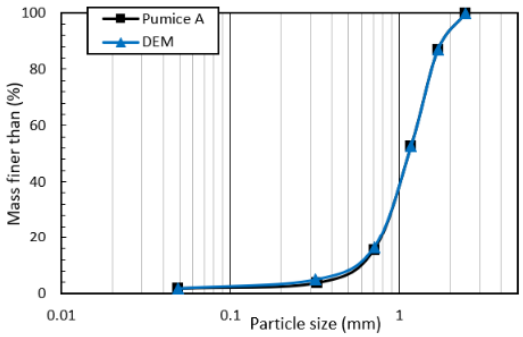

Figure 6: PSD curve for the pumice sand used in this simulation.

The results of the simulated tests based on the strain control method with 100 kPa confining pressure are shown in Figure 7. In addition, Figure 7 shows the results of a constant strain amplitude undrained triaxial test on the loose sample at a 4% strain amplitude level. The results are about the stress ratio attained a roughly constant value of 68 kPa on the compression phase and a value of 65 kPa on the extension phase. The reason for the difference in stress ratio between the compression and extension phases is due to the homogeneity of the DEM specimen. As observed from Figure 7, with application of constant strain amplitude, the deviator stress increases due to the decrease in the normalised mean effective stress, leading to the development of EPWP during testing. As the cyclic loading is applied, there is a gradual decrease in deviator stress on both the compression and extension phases. For the reason that reduction of deviator stress observed due to the EPWP development, a decrease of effective stress between the particles leads to a gradual decrease in the stiffness of the specimen. During the compression phase, the magnitude of deviatoric stress is greater than during the extension phase, as shown in Figure 7. The results of the normalised mean effective stress (p'/p_0) predicted by the numerical model are presented.

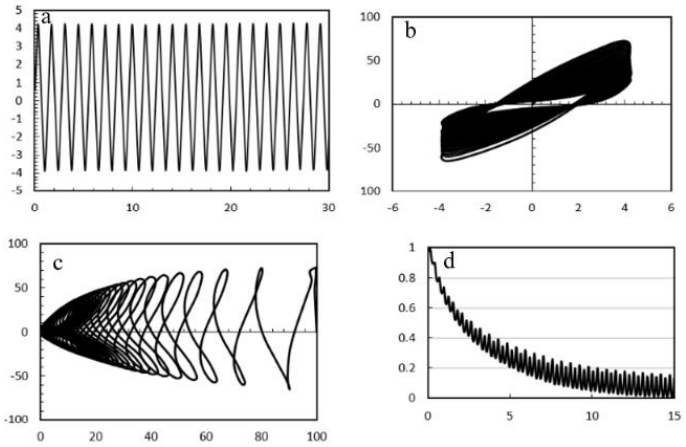

Figure 7: Results for 100 kPa confining pressure: (a) axial strain vs. number of cycles; (b) deviatoric stress vs. axial strain; (c) deviatoric stress vs. effective mean stress; and (d) $p'/p0$ vs. number of cycles.

In addition to the contact forces network, Figure 8 from the DEM results also provided other micro-level details, such as the evolution of particle crushing and mechanical coordination number. Although not shown here, the mechanical coordination number (indicating the average number of contacts a particle has) increases with axial strain as the particles are crushed during shearing, leading to the formation of new contacts. This behaviour is more evident under higher confining pressure.

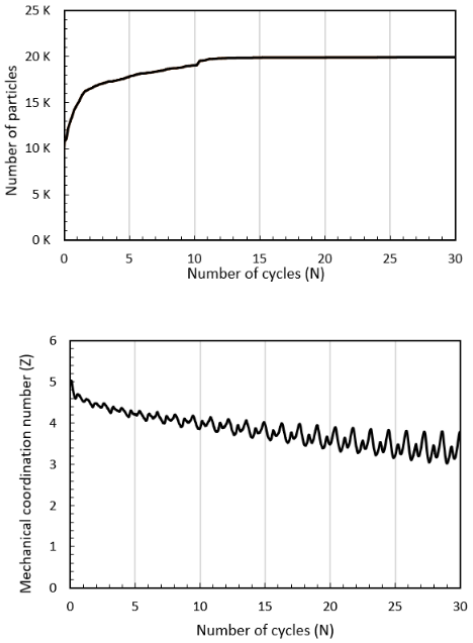

Figure 8: Results of the number of crushed particles and mechanical coordination number from the simulated cyclic undrained triaxial tests.

3.4 Evolution of pre- and post-PSD before and after cyclic undrained triaxial tests

To examine the impact of particle crushing during cyclic undrained triaxial test, the PSDs must be monitored during the simulations. The initial PSDs for the pumice specimen with 2 different states, loose and medium dense, under 100 kPa confining pressure are shown in Figure 9. After 250 cycles, the proportions of crushed particle sizes in the two samples in loose (Dr=30%) and medium dense (Dr=70%) states were similar, i.e. the proportion of smaller particles was significantly increased, and the proportion of larger particles was reduced.

Clearly, the loose specimen undergoes less particle crushing because there are many voids in the specimen that allow particles to rotate and rearrange, as compared with a medium-dense one, thereby limiting the number of crushed particles. On the other hand, the rotation and movement of particles in the medium-dense specimen are restricted by the adjacent particles due to fewer available voids, resulting in more particle crushing.

In addition, the results show that the number of crushed particles during the test with the two different confining pressures ($\acute{\sigma_c}$= 100 and 400 kPa) with the same cycles N >250 is different. The degree of particle crushing for the loose and the medium dense specimens tends to be different because of variations in confining pressure and density.

Moreover, another reason which affects the particle crushing during a particular range of cycles is due to the high EPWP development, besides the rearrangement between the crushed particles observed, as proved by Figure 10. However, the effect of confining pressure is significant, as an increase in confining pressure leads to a higher number of crushed particles.

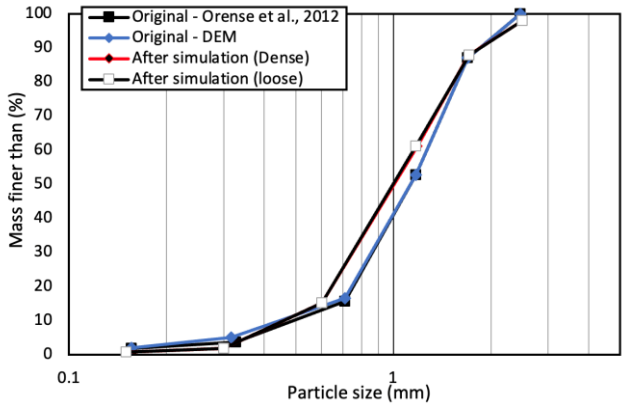

Figure 9: Initial PSD curves for pumice A sand and PSD after the experiment and DEM cyclic undrained triaxial test.

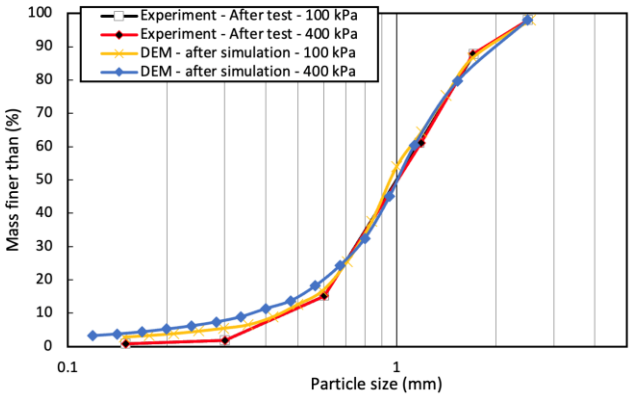

Figure 10: Comparison of PSD curves of loose pumice A sand specimen after 250 cycles in the experiment and simulated cyclic undrained triaxial test.

3.5 Crushed particles

Figure 11 shows the total number of particles that were generated in the loose and dense specimens after the initial 20 cycles due to crushing with cyclic strain (± 4%) applied under different confining pressures. The marks indicate that the total number of added particles increases nonlinearly with increasing number of cycles and confining pressure. Moreover, another factor that affects the number of general particles is related to the relative density of the specimen, the sizes of particles, and the number of cycles (cyclic loading). In terms of different relative densities, the rearrangement of particles after crushing affects the behaviour of the specimen due to the increase in the interaction.

The loose specimen underwent less particle crushing, whereas the particles in the dense specimen were restricted by the adjacent particles due to fewer voids available, resulting in more crushing when the testing was terminated after 20 cycles (Figure 11). The patterns in Figure 12, especially in cases with confining pressure between 200 and 500 kPa, indicate that the number of generated particles due to the crushing increases. To recall, the majority of the crushing occurred on the larger particles during the initial stage of testing.

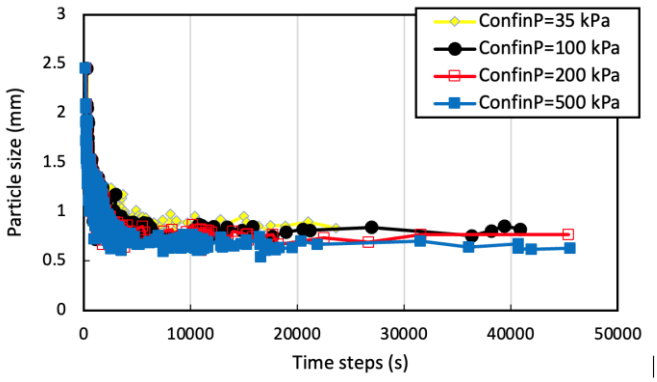

Figure 11: Comparison of the evolution of different particle sizes during the simulated cyclic undrained triaxial tests on loose (Dr =30%) pumice sand.

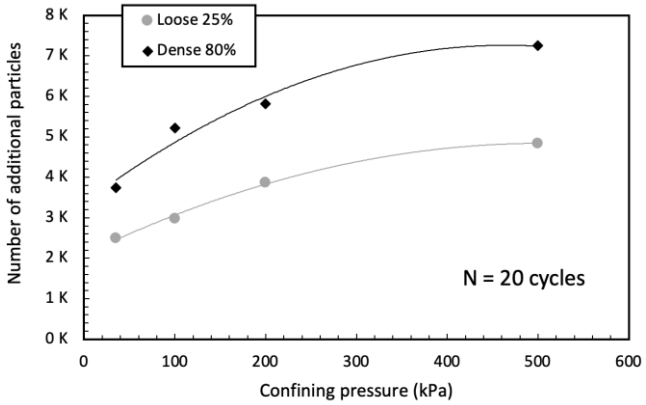

Figure 12: Total number of added particles after 20 cycles with controlled strain (±4%) for specimens with 25% and 80% relative density and different confining pressures.

For further study, the evolution of different particle sizes under various confining pressures (35 to 500 kPa) is presented in Figure 13. As seen, the size of crushed particles increases with increasing confining pressure for each test. The largest particles are crushed in the first step, which is the same as the observation during the single particle crushing test, and with increasing confining pressure, a larger number of small particles are crushed.

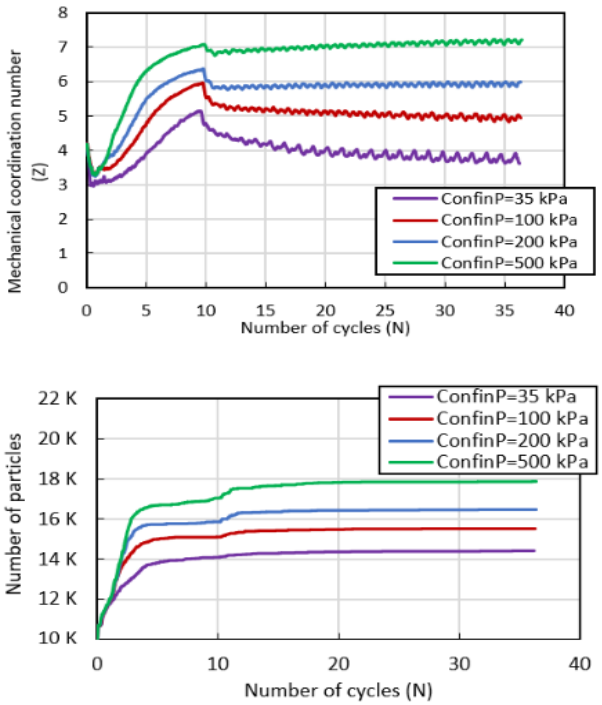

Figure 13: Results of simulated cyclic undrained triaxial compression tests of pumice sand for mechanical coordination number and number of particles vs. number of cycles.

4 CONCLUSIONS

- In this paper, the discrete element method (DEM) was employed to simulate the undrained cyclic triaxial test results of specimens comprising crushable pumice sands.
- The results of the simulations demonstrated that the developed DEM model, which incorporated the strong dependency of crushing strength on the particle size into the particle crushing criteria and complemented by the use of a non-linear contact model which considered rolling resistance, can generally capture the macro-behaviuor of pumice sand in monotonic triaxial conditions.
- Moreover, the DEM model provided opportunities to look at the micro-level response, such as the number of crushing vents and particle contacts, and the effect of confining pressure and specimen state condition during the cyclic testing process.

REFERENCES

[1] Belheine, N., Plassiard, J.-P., Donzé, F.-V., Darve, F. and Seridi, A. (2009): Numerical simulation of drained triaxial test using 3D discrete element modeling, *Computers and Geotechnics*, 36(1-2), 320-331. https://doi.org/10.1016/j.compgeo.2008.02.003

[2] Ciantia, M., Arroyo, M., Calvetti, F. and Gens, A. (2015): An approach to enhance efficiency of DEM modelling of soils with crushable grains, *Géotechnique*, 65(2), 91-110. https://doi.org/10.1680/geot.13.P.218

[3] Ciantia, M. O., Arroyo, M., O'Sullivan, C. and Gens, A. (2019): Micromechanical inspection of incremental behaviour of crushable soils, *Acta Geotechnica*, 14(5), 1337-

1356. https://doi.org/10.1007/s11440-019-00802-0
[4] Cil, M. B. and Alshibli, K. A. (2014): 3D analysis of kinematic behavior of granular materials in triaxial testing using DEM with flexible membrane boundary, *Acta Geotechnica*, 9(2), 287-298. https://doi.org/10.1007/s11440-013-0273-0
[5] Cundall, P. A. (1988): Formulation of a three-dimensional distinct element model—Part I. A scheme to detect and represent contacts in a system composed of many polyhedral blocks, *International Journal of Rock Mechanics and Mining Sciences & Geomechanics Abstracts*, 25(3), 107-116. https://doi.org/10.1016/0148-9062(88)92293-0
[6] Gong, G., Thornton, C. and Chan, A. H. (2012): DEM simulations of undrained triaxial behavior of granular material, *Journal of Engineering Mechanics*, 138(6), 560-566. https://doi.org/10.1061/(ASCE)EM.1943-7889.0000366
[7] Iwashita, K. and Oda, M. (1998): Rolling resistance at contacts in simulation of shear band development by DEM, *Journal of Engineering Mechanics*, 124(3), 285-292. https://doi.org/10.1061/(ASCE)0733-9399(1998)124:3(285)
[8] Kikkawa, N., Pender, M. J. and Orense, R. (2013): Comparison of the geotechnical properties of pumice sand from Japan and New Zealand, *Proceedings of the 18th International Conference on Soil Mechanics and Geotechnical Engineering* (pp. 239-242).
[9] Kumar, S. S., Krishna, A. M. and Dey, A. (2017): Evaluation of dynamic properties of sandy soil at high cyclic strains. *Soil Dynamics and Earthquake Engineering*, 99, 157-167. https://doi.org/10.1016/j.soildyn.2017.05.016
[10] McDowell, G. R. and Bolton, M. D. (1998): On the micromechanics of crushable aggregates, *Géotechnique*, 48(5), 667-679. https://doi.org/10.1680/geot.1998.48.5.667
[11] Orense, R. P., Pender, M. J. and O'Sullivan, A. S. (2012): *Liquefaction characteristics of pumice sands*, EQC Project Report 10/589, Earthquake Commission.
[12] Orense, R. P., Pender, M. J., Hyodo, M. and Nakata, Y. (2013): Micro-mechanical properties of crushable pumice sands, *Géotechnique Letters*, 3, 67-71. https://doi.org/10.1680/geolett.13.011
[13] O'Sullivan, C. (2011): *Particulate discrete element modelling: a geomechanics perspective*. CRC Press.
[14] Pender, M. J., Wesley, L. D., Larkin, T. J. and Pranjoto, S. (2006): Geotechnical properties of a pumice sand, *Soils and Foundations*, 46(1), 69-81. https://doi.org/10.3208/sandf.46.69
[15] Russell, A. R., Wood, D. M. and Kikumoto, M. (2009): Crushing of particles in idealised granular assemblies, *Journal of the Mechanics and Physics of Solids*, 57(8), 1293-1313. https://doi.org/10.1016/j.jmps.2009.04.009
[16] Šmilauer, V., Catalano, E., Chareyre, B., Dorofeenko, S., Duriez, J., Gladky, A., Kozicki, J., Modenese, C., Scholtès, L., Sibille, L and Stránský, J. (2010): Yade reference documentation, *Yade Documentation*, 474.
[17] Weibull, W. (1951): A statistical distribution function of wide applicability, *Journal of Applied Mechanics*, 18(3), 293-297. https://doi.org/10.1115/1.4010337
[18] Wesley, L. D., Meyer, V. M., Pranjoto, S., Pender, M., Larkin, T., & Duske, G. C. (1999): Engineering properties of a pumice sand, *Proceedings, 8th Australia New Zealand Conference on Geomechanics: Consolidating Knowledge* (Vol. 2, pp. 901-908). Australian Geomechanics Society.